Monochromatic-Tunable Terahertz-Wave Sources Based on Nonlinear Frequency Conversion Using Lithium Niobate Crystal

Koji Suizu and Kodo Kawase, *Member, IEEE*

(Invited Paper)

***Abstract*—We review widely tunable terahertz (THz)-wave generation by optical parametric processes using lithium niobate crystal. Applying the parametric oscillation of $LiNbO_3$ or a MgO-doped $LiNbO_3$ crystal pumped by a nanosecond Q-switched Nd:YAG laser, we realized coherent THz-wave sources with a simple configuration widely tunable in the range of 0.7–3 THz. For efficient coupling of the THz wave, we used a monolithic grating coupler or a Si-prism array coupler. In addition, Fourier transform limited THz-wave spectrum narrowing was achieved by introducing the injection seeding method. A line width of about 100 MHz (0.003 cm^{-1}) was assured by measuring the absorption spectrum of low-pressure water vapor. Using the difference frequency generating method with a periodically poled $LiNbO_3$ crystal, we achieved higher conversion efficiency and realized continuous THz-wave generation. This room temperature operated, tabletop system promises to be a widely tunable THz-wave source suited to a variety of applications.**

***Index Terms*—Difference frequency generation, lithium niobate, parametric frequency conversion, terahertz (THz) wave.**

I. Introduction

GREAT interest exists in the development of coherent terahertz (THz)-wave sources for use in applications such as low-frequency spectroscopy and biomedical analysis [1]. For high-resolution spectroscopy and other applications, a THz-wave source must be broadly tunable and possess a narrow spectral line width, and in the past two decades, a great deal of research has examined the generation of tunable coherent far-infrared radiation based on optical technology [2], [3]. The pioneering works of Pantell, Puthof, and others reported efficient, widely tunable THz generation in the late 1960s and early 1970s [4]–[6]. This was based on tunable light scattering from the long wavelength side of the A_1-symmetry softest mode in $LiNbO_3$. An input (pump) photon at near infrared stimulates a near-infrared Stokes photon (idler) at the difference frequency between the pump photon and the vibrational mode. Simultaneously, the parametric process generates a THz wave (signal) due to the nonlinearity arising from both the electronic and vibrational contributions of the material. The tuning is accomplished by controlling the propagation direction. Although the interaction is very efficient, most of the THz waves generated are absorbed or totally reflected inside the crystal due to its large absorption coefficient and high refractive index in the THz range. To allow THz radiation, a cut exit was made in the corner of the crystal. We devised an efficient, widely tunable source of coherent THz waves based on the principles presented in previous work, but with far better characteristics by introducing a monolithic grating coupler, an arrayed Si-prism coupler, doped crystals, and injection seeding.

The other way to generate THz waves via nonlinear optical down-conversion processes is difference frequency generation (DFG), a method that presents great advantages. This method facilitates tuning and yields wide tunability and high power output [7]–[9]. We also developed a novel source of coherent THz waves based on the DFG method and the quasi-phase-matching technique.

Manuscript received September 10, 2007; revised October 3, 2007. This work was supported in part by the Scientific Research (18206009) from the MEXT, in part by the Murata Science Foundation, in part by the Ministry of Internal Affairs and Communications of Japan under the Strategic Information and Communications R&D Promotion Program (SCOPE), in part by the Creative Scientific Research (13GS0002) from the MEXT, and in part by the Creative Scientific Research (17GS1204) from the MEXT.

K. Suizu is with the Department of Electrical Engineering, Nagoya University, Nagoya 464-8603, Japan (e-mail: suizu@nuee.nagoya-u.ac.jp).

K. Kawase is with the EcoTopia Science Institute, Nagoya University, Nagoya 464-8603, Japan. He is also with the RIKEN, Sendai 980-0845, Japan (e-mail: kawase@nuee.nagoya-u.ac.jp).

Digital Object Identifier 10.1109/JSTQE.2007.911306

II. THz-Wave Parametric Generation Using Polariton

A. Principles of Operation

The generation of coherent tunable THz waves results from the efficient parametric scattering of laser light via a polariton (stimulated polariton scattering). A polariton is a quantum of the coupled phonon–photon transverse wave field, and stimulated polariton scattering occurs when the pump excitation is sufficiently strong in polar crystals such as $LiNbO_3$, $LiTaO_3$, and GaP, which are both infrared- and Raman-active. The scattering process involves both second- and third-order nonlinear processes. Consequently, a strong interaction occurs among the pump, idler, and polariton (THz) waves. $LiNbO_3$ is one of the most suitable materials for generating THz waves efficiently because of its large nonlinear coefficient ($d_{33} = 25.2$ pm/V at $\lambda = 1.064$ μm [10], and estimated $d_{33} = 165$ pm/V at THz-wave region [26]) and its transparency over a wide wavelength range (0.4–5.5 μm). $LiNbO_3$ has four infrared- and Raman-active transverse optical (TO) phonon modes, called A_1-symmetry modes, and the lowest mode ($\omega_0 \sim 250$ cm^{-1}) is particularly useful for efficient tunable far-infrared generation

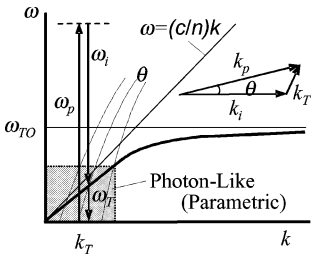

Fig. 1. Dispersion relation of the polariton, an elementary excitation generated by the combination of a photon and a transverse optical phonon ($\omega_{\rm TO}$). The polariton in the low energy region behaves like a photon at THz frequency. Due to the phase-matching condition as well as the energy conservation law, which hold in the stimulated parametric process, tunable THz wave is obtained by the control of the wavevector $\boldsymbol{k}_T$. The inset shows the noncollinear phase matching condition.

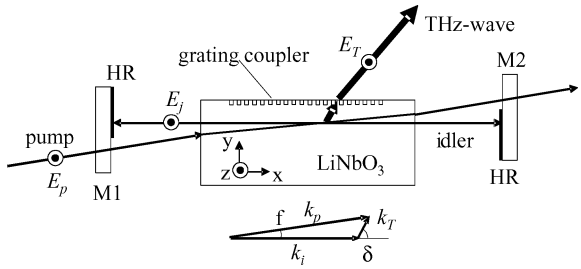

Fig. 2. Experimental cavity arrangement for the TPO using a monolithic grating coupler on the y-surface of the $LiNbO_3$ crystal.

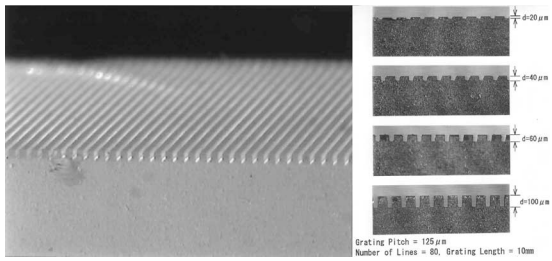

Fig. 3. Magnified view of the grating coupler formed on the y-surface of $LiNbO_3$ crystal.

because it has the largest parametric gain, as well as the smallest absorption coefficient [11].

The principle of tunable THz-wave generation is as follows. Polaritons exhibit phonon-like behavior in the resonant frequency region (near the TO-phonon frequency $\omega_{\rm TO}$). However, they behave like photons in the nonresonant low-frequency region (Fig. 1), where a signal photon at THz frequency (ω_T) and a near-infrared idler photon (ω_i) are created parametrically from a near-infrared pump photon (ω_p), according to the energy conservation law $\omega_p = \omega_T + \omega_i$ (p: pump, T: THz, i: idler). In the stimulated scattering process, the momentum conservation law $\boldsymbol{k}_p = \boldsymbol{k}_i + \boldsymbol{k}_T$ (noncollinear phase-matching condition; see the insets of Fig. 1) also holds. This leads to the angle-dispersive characteristics of the idler and THz waves. Consequently, a coherent THz wave is generated efficiently by using an optical resonator for the idler wave, and continuous, wide tunability is accomplished simply by changing the angle between the incident pump beam and the resonator axis.

B. THz-Wave Parametric Oscillator With a Monolithic Grating Couple

This method uses a single-fixed optical source, and is performed at room temperature. The idler (Stokes) and signal (THz) waves are generated from the pump (near infrared) wave in the direction consistent with the noncollinear phase-matching condition inside the $LiNbO_3$ crystal; the idler wavelength is a few nanometers longer than the pump wavelength. A widely tunable coherent THz wave is generated easily by slightly changing the incident angle of the pump beam. The nonlinearity arises from both the electronic and vibrational contributions of the material. Although the interaction between waves is generated by stimulated oscillation, most of the generated THz wave is absorbed or totally reflected inside the crystal due to the large absorption coefficient and refractive index of the material (5.2 in the THz range [12]). Therefore, it is difficult to couple out the THz radiation efficiently to the free space. One study [6] used a specially prepared crystal in which one corner was cut and polished at the proper angle to allow the THz radiation to emerge approximately normal to the exit surface, avoiding the problem of total internal reflection. In this paper, we used a grating structure on the surface of the $LiNbO_3$ to couple out the THz wave to the free airspace directly with almost 1000 times greater efficiency [13], [14].

Our experimental setup is shown in Fig. 2. A 3.5-mm-thick $LiNbO_3$ z-plate was cut to $50 \times 10 \times 3.5(x \times y \times z)$ mm^3. The two end-surfaces in the x-plane were cut parallel, polished, and antireflection (AR) coated for operation at 1.07 μm. The grating coupler was fabricated on the y-surface by precise machining using a cutter (DAC-2SP/86; Disco, Tokyo, Japan), as shown in Fig. 3, and the grating pitch and length were 125 μm and 10 mm, respectively. Four different depths of grating were formed on the sample: 20, 40, 60, and 100 μm. The crystal was placed inside the 15-cm-long cavity, as shown in Fig. 2, and was resonated by the idler wave using two high-reflection (HR) mirrors: M1 ($f = \infty$) and M2 ($f = 10$ m). Both mirrors were half-area coated, so that only the idler wave could resonate and the pump beam propagated through the uncoated area without scattering. The mirrors and crystal were mounted on a rotating stage and tuned by rotating the stage slightly to vary the angle of the resonator with respect to the pump wave. The pump source was a Q-switched Nd:YAG laser (SOLAR, LF113, 1.064 μm) whose electric field was along the z-axis of the crystal. The pump power, pulse width, and repetition rate were 30 mJ/pulse, 25 ns, and 16.7 Hz, respectively. The pump beam entered the x-surface of the $LiNbO_3$ crystal and passed through it close to the surface of the grating coupler to minimize the absorption loss of the THz radiation ($\alpha > 10$ cm^{-1}) [12]. Near-infrared idler oscillation around 1.07 μm was clearly recognized by the oscillating spot above a threshold pump power density of about 130 mW/cm^2. The THz-wave radiation was monitored with a 4 K Si bolometer (Infrared Laboratories, Tucson, AZ). To suppress its response to infrared regions, a Yoshinaga filter was installed inside. A white polyethylene lens ($f = 60$ mm) was set in front of the bolometer to focus the THz-wave radiation.

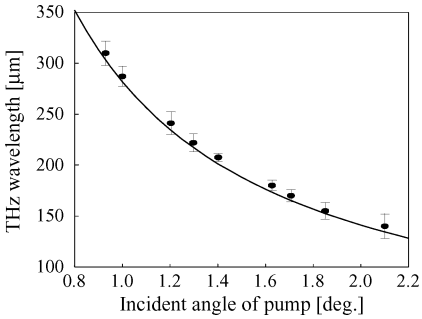

Fig. 4. Tuning characteristic between the incident angle of the pump to the x-surface of the crystal normal, generated THz wavelength. Solid curve indicates the calculated tuning curve.

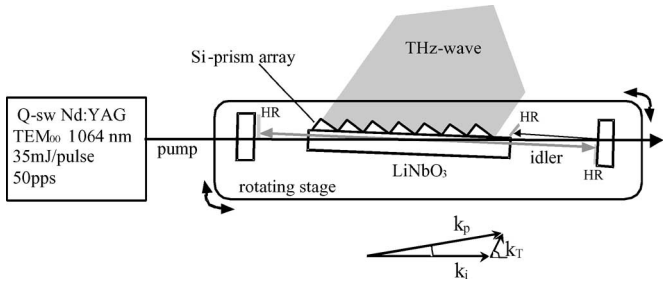

Fig. 5. TPO with a Si-prism array. The Si-prism array was introduced to increase the output, and to reduce the diffraction angle of the THz wave by increasing the coupling area. An array of seven right-angle Si-prism couplers was placed on the y-surface of the $LiNbO_3$. The total base length was 8 mm $\times$ 7 $=$ 56 mm.

A Schottky barrier diode [15] was used to detect the temporal characteristic of THz waves with a time response faster than 10 GHz. Simultaneously, the intensity of the idler was measured using a power meter and recorded together with the bolometer output in a computer via a digital oscilloscope.

As shown in the inset of Fig. 2, the THz wave was generated in the direction satisfying the noncollinear phase-matching condition. Here, k_j is the wave vector with $j = p$, i, and T, indicating the pump, idler, and THz waves, respectively. As the relationship $k_p > k_i \gg k_T$ holds, angle ϕ between the pump and idler waves is small ($\phi \approx 1^\circ$), while angle δ between the idler and THz wave is large ($\delta \approx 65^\circ$).

By varying the incident angle of the pump beam from 2.1° to 0.9°, angle ϕ between the pump and the idler inside the crystal was changed approximately from 1° to 0.5°. As the phase-matching angle changed, the idler and the THz wavelength were tuned from 1.072 to 1.068 μm and from 140 to 310 μm, respectively, as depicted in Fig. 4. Angle δ between the THz and the idler inside the crystal changed from 66° to 65°. We also found that $LiTaO_3$ was capable of oscillating in the same cavity. With $LiTaO_3$, we needed to make the incident angle of the pump larger than that with $LiNbO_3$.

For the 25 ns pulse width of the pump wave, the pulse widths of the idler and THz waves were about 10 ns. Hence, the THz wave consisted of several tens of thousands of cycles during the oscillation time, so that the coherency was sufficient. The THz wavelength and line width were measured using a scanning Fabry–Pérot etalon consisting of two Ni metal mesh plates with a 65 μm grid. The free spectral range (FSR) of the etalon was about 100 GHz, and the measured line width was almost 20 GHz. Using a wire grid polarizer, the measured polarization of the THz wave was parallel to the z-axis of the crystal, coinciding with those of the pump and idler waves. The measured peak THz-wave output from a 10-mm-long grating coupler was 3 mW with a pump power of 34.5 mJ/pulse. Accordingly, we could obtain almost 15 mW of output peak power from the grating coupler over the entire y-surface of the 50-mm-long crystal. When we also made a cut exit at the end corner of the crystal, we obtained only 5 μW of peak power at best, under the same conditions. In comparison to the cut exit, the grating coupler had an efficiency of more than $\times$1000. Furthermore, almost 100 times greater THz-wave output was obtained by cooling the crystal to liquid nitrogen temperature [16].

The intensity distribution of the generated beam was Gaussian-like both along and perpendicular to the grating. Full-width at half-maximum (FWHM) spot sizes of 8 and 12 mm were observed along the grating direction (x) at the measured points 150 and 300 mm from the grating, which corresponded to a beam divergence of 0.8°. Along the z-axis, the divergence was determined by the pump spot size to be 1.5°. These results are in good agreement with diffraction theory.

C. Arrayed Si-Prism Coupler for a THz-Wave Parametric Oscillator

We introduced a Si-prism coupler ($n \approx 3.4$) to extract the THz wave generated inside a nonlinear crystal, thereby substantially improving the exit characteristics [17]. This section describes the characteristics of the oscillation, and a novel coupling method for THz waves using an arrayed Si prism [18]. Applying the arrayed-prism coupler, a sixfold increase in the coupling efficiency and a 40% decrease in the far-field beam diameter are achieved compared to using a single-prism coupler. We also discuss the negative effect of the free carriers at the Si-prism surface excited by the scattered pump beam, and the positive effect of cavity rotation on the unidirectivity of THz-wave radiation from the Si prism.

The basic configuration of the source consisted of a Q-switched Nd:YAG laser (LS-2136, 1.064 μm; LOTIS, Tokyo, Japan) and a parametric oscillator, as shown in Fig. 5. The $LiNbO_3$ crystal used in the experiment was cut from a 5 $\times$ 65 $\times$ 6 mm^3 wafer (thick $\times$ x $\times$ y). The x-surfaces at both ends were mirror polished and AR coated. The y-surface was also mirror polished to minimize the coupling gap between the prism base and crystal surface, and to prevent scattering of the pump beam, which excites a free carrier at the Si-prism base. The pump wave passed through the crystal close to the y-surface to minimize the travel distance of the THz wave inside the crystal. The idler wave was amplified in an oscillator consisting of flat mirrors with half-area HR coating. In the experiment, the beam diameter, pulse width, and repetition of the pump wave were 1.5 mmϕ, 25 ns, and 50 Hz, respectively, and the typical excitation intensity was 30 mJ/pulse. The mirrors and crystal were installed on a precise, computer-controlled rotating stage (Nanoradian Stage; Harmonic Drive Systems, Hauppauge, NY) for precise tuning.

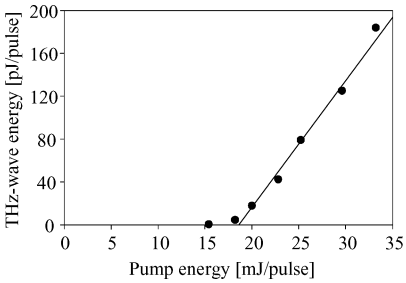

Fig. 6. Typical input–output characteristics of an TPO with a Si-prism array. By increasing the prism base area, the THz-wave output to more than six times that of a single-prism coupling was obtained.

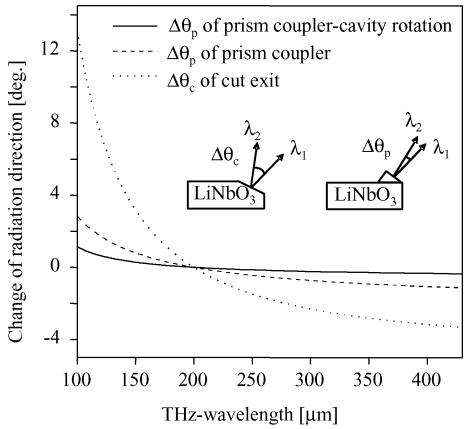

Fig. 7. Calculated radiation angle changes for two different THz coupling methods: cut exit and Si-prism coupler. The dotted and broken lines indicate the radiation angle changes for the cut exit $\Delta\theta_c$ and Si prism coupler $\Delta\theta_p$, respectively. The solid line shows the actual change in THz-beam direction when observed from outside the TPO. Since the TPO cavity can be angle tuned by rotating the stage in the direction counter to $\Delta\theta_p$, the actual angle change becomes much smaller than $\Delta\theta_p$. The changes in the radiation angle are set at zero for $\lambda_{\mathrm{THz}} = 200\ \mu$m, for comparison.

A Si-prism array was introduced to obtain higher THz-wave output by increasing the coupling area. An array of seven Si-prism couplers was placed on the y-surface of the $LiNbO_3$, as shown in Fig. 5. The right-angle prisms were fabricated from high-resistivity Si ($\rho > 1\ \mathrm{k}\Omega \cdot \mathrm{cm}$, $\alpha \cong 0.6\ \mathrm{cm}^{-1}$); each was cut from a bulk Si crystal using a precise diamond cutter to dimensions of $8.0 \times 6.1 \times 5.1 \times 5.0$ mm (base $\times$ face $\times$ side $\times$ thickness), and the angles were 50°, 40°, and 90°, respectively. The total base length was 8 mm $\times\ 7 = 56$ mm. A prism opening angle of $\xi = 40°$ was chosen so that the THz wave would emerge almost normal to the prism face ($6.1 \times 5.0\ \mathrm{mm}^2$). To maximize the coupling efficiency, the base of the prisms was pressed against the y-surface of the $LiNbO_3$ crystal using a specially designed holder.

The typical input–output characteristics of a THz-wave parametric oscillator (TPO) with a Si-prism array are shown in Fig. 6, in which the oscillation threshold was 18 mJ/pulse. With a pump power of 34 mJ/pulse, the THz-wave output from the prism array was 192 pJ/pulse ($\cong$ 19.2 mW at the peak), calibrated using the sensitivity of the bolometer. Since the Si-bolometer output becomes saturated at approximately 5 pJ/pulse, we used several sheets of thick paper as an attenuator after calibration. The minimum sensitivity of the Si bolometer is approximately 1 fJ/pulse; therefore, the dynamic range of measurement using the TPO as a source is 192 pJ/fJ, which exceeds 50 dB. In the case of single-prism coupling, the typical output was about 30 pJ/pulse (3 mW at the peak) at best under similar conditions, i.e., a THz wavelength of 180 μm and idler output of 1 mJ/pulse. In comparison, the prism array was capable of emitting more than six times more THz-wave energy than the single-prism coupling due to the seven-times-wider base area.

A small portion of the pump beam was reflected from the end mirror or scattered at the crystal edge and shone on the emitting face of the Si prism, generating a free carrier that strongly absorbed the THz wave. Therefore, an HR mirror was installed in front of the last Si prism to intercept the reflected pump beam, as illustrated in Fig. 5. The HR mirror needed to be close to the y-surface of the $LiNbO_3$ crystal to intercept the pump beam, as a pump of only 10 $\mu\mathrm{J/cm}^2$ is sufficient to generate the free carrier in Si [19]. Without the HR mirror, the THz-wave output from the last Si prism decreased between 10^{-2} and 10^{-3} of the output with the HR mirror in place. Given the difficulty in shielding the scattered pump perfectly, it was difficult to obtain the maximum THz-wave output (~3 mW at the peak) using a single-prism coupling, even with the HR mirror. In comparison, it was much easier to extract the maximum THz-wave output (~20 mW at the peak) from the arrayed prism because the last prism acts as a perfect auxiliary shield for the scattered pump.

The spatial intensity distribution of the THz-wave radiation was measured by shifting a Si bolometer with a 1.4-mm-wide incident slit transversely. The beam pattern and diffraction of the THz wave in the z-plane were measured for the single- and arrayed-prism couplers. The distance between the prism coupler and the slit is indicated as d. In both measurements, the THz wavelength was 170 μm, and the angle between the THz beam and y-surface of the crystal was 50°. With the single-prism coupling, both the near- and far-field patterns were Gaussian-like, and the measured diffraction angle in the far field was 1.4°. With the arrayed-prism coupling, the far-field pattern was almost Gaussian-like, whereas the near-field pattern was asymmetric. In the near field, higher output was observed from the prisms closest to the pump exit surface because as the distance between the pump and the y-surface of the crystal shortened, the absorption loss of the THz wave decreased. The output of each prism was distinguishable at $d < 10$ cm, whereas the beam pattern became continuous at $d > 20$ cm. The diffraction angle of the THz wave emitted from the prism array coupler was apparently smaller than that of the single-prism coupling, comparing the FWHM of the beam pattern at a distance of $d = 100$ cm. At $d = 100$ cm, the FWHM was 58 mm for the single-prism coupling and 34 mm for the arrayed-prism coupling. The far-field diffraction angle was determined by the emitting aperture width and wavelength. The smaller diffraction angle was obtained with the prism array due to the seven-times-wider emitting aperture compared to the single prism.

In previous experiments [6], a cut exit was used to avoid the total internal reflection, as illustrated in Fig. 7. The cut exit was made at the corner of the $LiNbO_3$ crystal, so that the THz

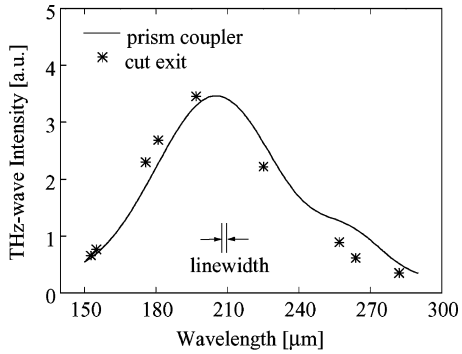

Fig. 8. Measured THz-wave intensity dependence on the wavelength for prism coupler (solid line) and cut exit (stars). In the case of prism coupler, the bolometer position was fixed, meanwhile, in the case of cut exit, the bolometer position had to be shifted point to point each time to measure, since the radiation angle varied as it tuned.

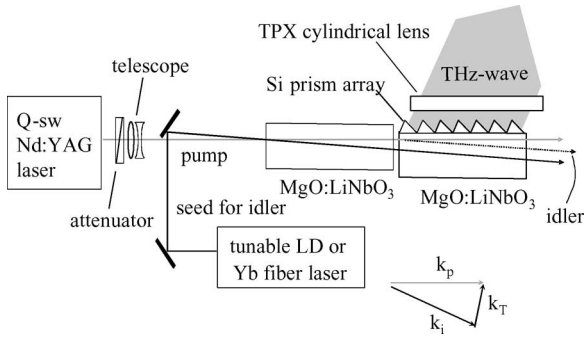

Fig. 9. Setup used for our experimental IS-TPG. The pump was a single longitudinal mode Q-sw Nd:YAG laser (1.064 μm), and the seed for the idler was a continuous-wave Yb-fiber laser (1.070 μm) or tunable laser diode (1.066–1074 μm).

wave emerged approximately normal to the exit surface. In this case, the refractive index dispersion of $LiNbO_3$ and change in the phase-matching angle δ directly influenced the THz-wave direction change $\Delta\theta_c$. Conversely, when a Si-prism coupler was used, the radiation went almost all in one direction, and the variation in the phase-matching angle was reduced substantially. Fig. 7 shows the calculated changes in radiation angle for these two methods of coupling. The changes in the radiation angle were set at zero for $\lambda_{\mathrm{THz}} = 200$ μm for comparison. The dotted and broken lines indicate the changes in the radiation angle for the cut exit $\Delta\theta_c$ and the Si-prism coupler $\Delta\theta_p$, respectively. The solid line shows the change in THz-beam direction when observed from outside the TPO. Note that since the TPO cavity can be angle tuned by rotating the stage in the direction counter to $\Delta\theta_p$, the actual angle change becomes much less than $\Delta\theta_p$. For the tuning range of 100–420 μm, $\Delta\theta_c = 16.5^\circ$, $\Delta\theta_p = 4.0^\circ$, and the actual change $\Delta\theta_p$ − (cavity rotation) $= 1.5^\circ$.

An example of the tuning range using the Si prism is shown in Fig. 8 as the solid line. In the figure, asterisks ($*$) indicate the data obtained with the cut exit at the end corner of the $LiNbO_3$ crystal. With the cut exit, the bolometer position had to be shifted for each measurement, since the radiation angle varied as the setup was tuned. On comparing the tuning ranges of both methods, we obtained an essential constant radiation direction by using the Si prism.

D. Injection-Seeded THz-Wave Parametric Generator (IS-TPG)

Coherent tunable THz waves were generated successfully using an injection-seeded THz-wave parametric generator (IS-TPG) based on laser light scattering from the A_1-symmetry polariton mode of MgO:$LiNbO_3$ crystals. The THz-wave spectrum was narrowed to the Fourier transform limit by injection seeding the idler wave (near-infrared Stokes). This resulted in a THz-wave output approximately 300 times greater than that of a conventional TPG that has no injection seeder. In addition, wide tunability from 0.7 to 2.4 THz was achieved using a tunable diode laser as the injection seeder. A resolution of less than 100 MHz (0.003 cm^{-1}) was assured by the absorption spectrum measurement of low-pressure water vapor. This compact system operates at room temperature and promises to be a new, widely tunable THz-wave source.

We investigated a TPO and TPG using $LiNbO_3$ or MgO:$LiNbO_3$ crystals. The TPO has proven to be a useful coherent THz-wave source that operates at room temperature. It is continuously tunable in the range of 1–3 THz in one operation and can emit peak powers of up to several tenths of a milliwatt. The difference between a TPO and a TPG is that the former has an idler cavity, while the latter does not. The THz-wave line width of a conventional TPG exceeds 500 GHz, and the THz-wave output is much smaller than that from a TPO. Therefore, we previously concentrated our efforts on the development of a TPO system, although its line width was tens of gigahertz.

This section is primarily concerned with work on TPGs, which appear to perform better than TPOs. The TPG spectrum was narrowed to the Fourier transform limit of the pulse width by introducing injection seeding to the idler [20]–[22]. The purity of the THz-wave frequency was improved dramatically to $\Delta\nu/\nu < 10^{-4}$. Simultaneously, the output obtained was several hundred times greater than that of a conventional TPG. In addition, wide tunability and fine resolution were demonstrated using a tunable seeder. Even in the optical region, injection seeding to a nanosecond optical parametric generator (OPG) has not been reported until recently [23] due to the limit of parametric gain.

Fig. 9 shows the setup of our experimental injection-seeded TPG. Arrangements were tested using one, two, and three 65-mm-long nonlinear crystals. The maximum THz-wave output was obtained when two crystals (5 mol% MgO-doped $LiNbO_3$) were used in series. The TPG efficiency of MgO:$LiNbO_3$ is several times higher [11] than that of non-doped $LiNbO_3$. Both crystals were cut into $65 \times 6 \times 5$ mm $(x \times y \times z)$ pieces. The x-surfaces were polished and AR coated. An array of seven Si-prism couplers was placed on the y-surface of the secondary MgO:$LiNbO_3$ crystal for efficient coupling of the THz wave, as shown in Fig. 9. The pump used was a single longitudinal mode (SLM) Q-switched Nd:YAG laser (SL404 T, wavelength: 1.064 μm, energy: <50 mJ/pulse, pulse width: 15 ns, beam profile: TEM_{00}; Spectron, Tokyo, Japan). To increase the power density, the pump beam diameter was decreased to 0.8 mmϕ using a telescope. The pump

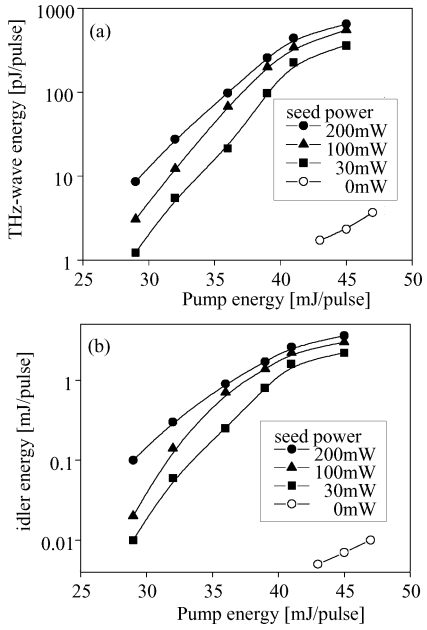

Fig. 10. Input–output characteristics of an IS-TPG, showing energy enhancement of the (a) THz wave (190 μm) and (b) idler (1.070 μm) by a factor of several hundreds with injection seeding.

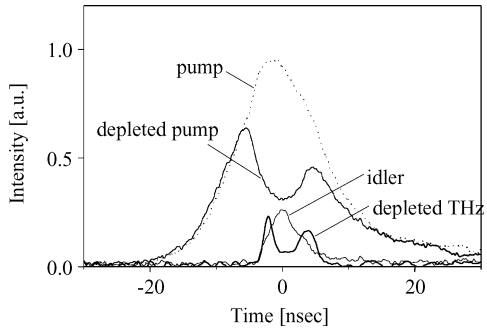

Fig. 11. Temporal waveforms of the pump (1.064 μm), idler (1.07 μm), and THz wave (190 μm). The pump energy was 45 mJ and the seed power was 250 mW. This is the largest pump depletion (28.4%) observed during our research on TPGs and TPOs.

power density was $<$530 mW/cm^2 at the crystal surface and could be varied with an attenuator. The pump beam was almost normal to the crystal surfaces as it entered the crystals and passed through the crystal close to the y-surface. A continuous wave (CW) SLM Yb-fiber laser (wavelength: 1.070 μm fixed, power: $<$300 mW) or tunable diode laser (wavelength: 1.066–1.074 μm, power: 50 mW) was used as an injection seeder for the idler. Observation of the intense idler beam easily confirmed the injection-seeded THz-wave generation. The polarizations of the pump, seed, idler, and THz waves were all parallel to the z-axis of the crystals. The THz-wave output and temporal waveform were measured with a 4 K Si bolometer and a Schottky barrier diode detector, respectively.

Energy enhancement of the THz and idler waves by injection seeding is shown in Fig. 10(a) and (b), respectively. The THz and idler outputs are roughly proportional to each other. Comparison of the output from the 0 and 200 mW seeding enabled us to determine that the THz wave and idler energies increased by factors of nearly 300 and 500, respectively. The maximum conversion efficiency was achieved when the pump and seed beams overlapped almost completely at the incident surface of the first MgO:LiNbO$_3$ crystal, as shown in Fig. 9. This was confirmed by the fact that initial excitation is an essential feature of injection seeding. The maximum THz-wave output of 900 pJ/pulse (peak $>$ 100 mW) was obtained with a pump of 45 mJ/pulse and a seed of 250 mW. In our previous studies, the maximum THz-wave output from a conventional TPG and a TPO was 3 and 190 pJ/pulse, respectively [18]. Because the Si bolometer became saturated at about 5 pJ/pulse, we used several thick calibrated papers as an attenuator. As the minimum sensitivity of the Si bolometer was almost 1 fJ/pulse, the dynamic range of the injection-seeded TPG system was 900 pJ to 1 fJ $\sim$ 60 dB, which is sufficient for most applications. The dynamic range can be increased significantly using a lock-in amplifier.

The outputs began to saturate with a seed power of almost 100 mW. A relatively high-seed power was required in this experiment because the seed energy did not contribute fully to idler generation. The seed and idler beams were separated from each other spatially because the pump and seed beams were separated spatially inside the secondary MgO:LiNbO$_3$ crystal, and because most of the idler energy was generated inside the secondary MgO:LiNbO$_3$ crystal. When one crystal was used, 10 mW of seed power was sufficient to obtain idler saturation because the pump and seed beams were not separated. Therefore, it is important to somehow confine the pump and seed beams in a long interaction volume to decrease the required seed power and to increase the efficiency. The angle between the idler beam and crystal x-surface normal was almost 1.5°, verifying that the cavity effect of the crystal surfaces has no relation to this parametric generation.

Fig. 11 shows examples of temporal waveforms of the pump, idler, and THz wave using a pump energy of 45 mJ and a seed power of 250 mW. The pulse widths of the pump and idler were 15 and 4 ns, respectively. The observed pump depletion (28.4%) was the largest depletion encountered during our TPG/TPO research. The THz waveform was also found to be depleted, probably due to back conversion of the pump. The second peak of the pump waveform in Fig. 11 was due to back conversion, and the product of $E_p \times E_i$ resulted in the second peak of the THz waveform. The depletion of the THz waveform was not observed with pump energies below 35 mJ/pulse. The THz waveform began to deplete as the pump energy increased, although the THz-wave energy continued to increase due to the pulse width expansion.

The THz-wave beam pattern was measured at a distance of about 40 cm from the Si-prism array. The beam pattern was nearly Gaussian and had a diameter of 7 mmϕ, which is suitable for many applications. The original vertical divergence was about 6°, as determined from the pump beam diameter and the wavelength according to diffraction theory. A cylindrical lens ($f = 30$ mm) made of polymethylpentene (PMP or 'TPX') was used, as shown in Fig. 9, to collimate the THz-wave divergence in the vertical (z-axis) direction. For the horizontal direction, the

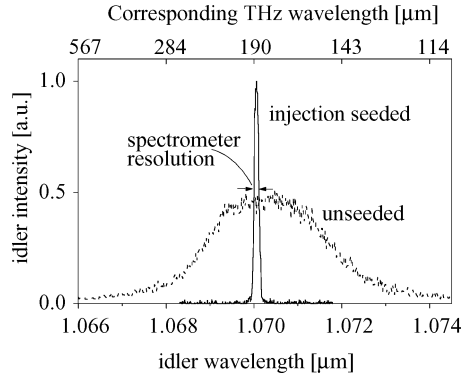

Fig. 12. Narrowing of the idler (1.07 μm) spectrum by injection seeding. The dotted and solid lines indicate the idler spectrum of a conventional TPG and an IS-TPG, respectively. The resolution limit of the spectrum analyzer used was 0.2 nm, so the real idler linewidth was much narrower than in this figure.

beam diameter decreased as it propagated due to the phased-array-like effect of the Si-prism array [18]. Furthermore, the THz beam can be focused tightly onto a spot of about 0.5 mmϕ using a short focus TPX or Si lens.

Fig. 12 shows the effect of injection seeding on idler spectrum narrowing. The dotted line indicates the idler spectrum of a conventional TPG without injection seeding, and the solid line denotes the idler spectrum of an injection-seeded TPG. The resolution limit of the spectrum analyzer used was 0.2 nm, so the real idler spectrum was much narrower than shown in this figure. Using a solid etalon, the idler spectrum was assured to be less than 1 GHz.

The THz wavelength and line width were measured using a scanning Fabry–Pérot etalon consisting of two Ni metal meshes with a 65 μm grid. Fig. 13 shows the transmitted THz-wave power as a function of etalon spacings of 1) about 80 and 2) about 210 mm. Fig. 13(a) demonstrates the stability of the spectrum and output during the 20 min scan. The displacement between the two periods (190 μm) corresponds to the wavelength directly. The merit of an injection-seeded TPG lies in its output stability due to the mode-hop-free characteristic, since it has no cavity. Conversely, as with an injection-seeded TPO [24], the cavity length must be controlled actively to match the seed wavelength to stabilize the output. In Fig. 13(b), the free spectral range (FSR) of the etalon was 750 MHz, and the measured THz-wave line width was less than 200 MHz $(0.0067\ \mathrm{cm}^{-1})$, which is our measurement resolution limit. Since the etalon spacing was up to 210 mm, the THz-wave pulse (3.4 ns) made less than three round trips in the etalon cavity, and thus, the resolution was inevitably limited.

The Fourier transform limit of the spectral width was calculated from the pulse shape of the THz wave as measured with the Schottky barrier diode. The typical pulse width of the THz wave was 3.4 ns, and was almost identical to that of the idler, which was measured with a high-speed photodetector. The calculated line width was 136 MHz. In this calculation, we ignored any fluctuations in the background noise near the zero level. These facts confirmed that the line width of the THz wave was narrowed to near the Fourier transform limit. The THz-wave line

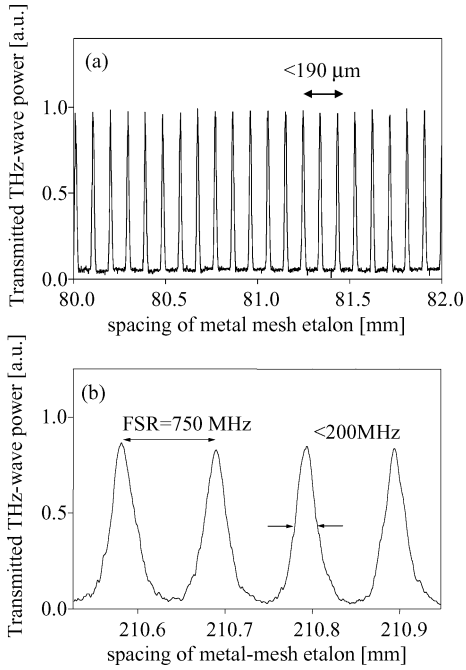

Fig. 13. THz linewidth and wavelength measured with a scanning Fabry–Perot etalon consisting of two metal-mesh plates. (a) Stability of the spectrum is demonstrated and the displacement between the two periods (190 μm) corresponds directly to the wavelength. (b) FSR of the etalon is 750 MHz and the linewidth of the THz wave is measured to be less than 200 MHz $(0.0067\ \mathrm{cm}^{-1})$, which is our measurement resolution limit.

width still exceeded 10 GHz, even with an injection-seeded TPG that used a multifrequency Nd:YAG laser as the pump. Therefore, both the pump and seed must be SLM lasers to obtain a transform-limited THz wave with a TPG.

It was possible to tune the THz wavelength using an external cavity laser diode as a tunable seeder. The wide tunability from 125 to 430 μm (frequency: 0.7–2.4 THz, wave number : 23–80 cm^{-1}) was achieved by changing both the seed wavelength and seed incident angle, as shown in Fig. 14. Squares and circles indicate the tunability of the THz and idler waves, respectively. In this experiment, both crystals were MgO:$LiNbO_3$. The wavelength of 430 μm (0.7 THz) was the longest ever observed during our studies on TPGs and TPOs. In the longer wavelength region, the angle between the pump and idler becomes less than 1°, so it is difficult for the TPO to oscillate only the idler inside the cavity without scattering the pump. In the shorter wavelength region, the THz output is comparatively smaller than the idler output due to the larger absorption loss inside the crystal.

The absorption spectrum of low-pressure ($<$1 Torr) water vapor was measured to demonstrate the continuous tunability and high resolution of the IS-TPG. The absorption gas cell used was an 87-cm-long stainless steel light pipe with TPX windows at both ends. Fig. 15 shows an example of measurements at around 1.92 THz, where two neighboring lines exist. The resolution was clearly less than 100 MHz $(0.003\ \mathrm{cm}^{-1})$. In fact, it is difficult for Fourier transform infrared spectrometers in the THz-wave region to have a resolution better than 0.003 cm^{-1} because of the instability of the scanning mirror for more than a meter. The system is capable of continuous tuning at high spectral

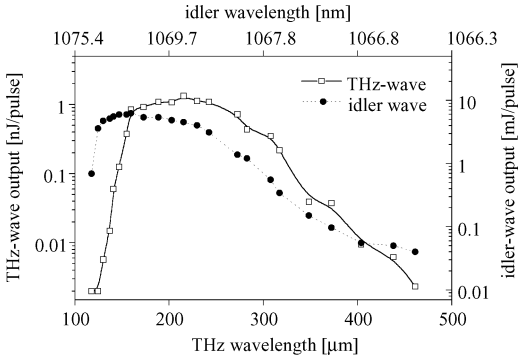

Fig. 14. Wide tunability of an injection-seeded TPG. Squares and circles indicate the tunability of the THz and idler waves, respectively.

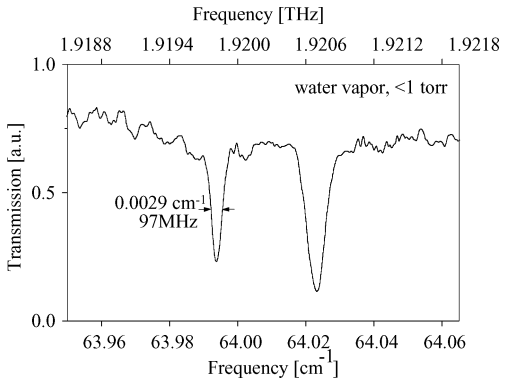

Fig. 15. Example of the absorption spectrum measurement of low-pressure ($<$1 torr) water vapor at around 1.919 THz. Resolution of less than 100 MHz (0.003 cm^{-1}) was clearly shown.

resolution in 4 GHz segments anywhere in the 0.7–2.4 THz region. The range of continuous tuning is currently restricted by the mode hop of the tunable laser diode. Since no cavity exists to be slaved, continuous tuning is extendible, in principle, to the full tunability of the IS-TPG by using a mode-hop-free seeder, such as a Littman-type external cavity diode laser.

We next measured the change in THz-wave output as a function of the seed incident angle. In this experiment, the seed (1.07 μm) and THz (190 μm) wavelengths were fixed, and the calculated noncollinear phase-matched angle was 1.43°. Here, it was important for the injection seeding to not be overly sensitive to the seed incident angle. In addition, the line width was assured to be less than 200 MHz at any deviated incident angle. From this, we see that continuous tuning is possible, to an extent, by simply varying the seed wavelength without having to adjust the incident angle. In practice, the tuning was obtained without changing the seed incident angle. Tuning without mechanical movement will lead to a stable, compact spectroscopic system. Even when the incident angle must be varied for wide tuning, such as in Fig. 15, no requirement exists to control the angle due precisely to this tolerance. In contrast, as with the injection-seeded TPO [24], the incident angle must be controlled precisely so that it is always perpendicular to the cavity mirror.

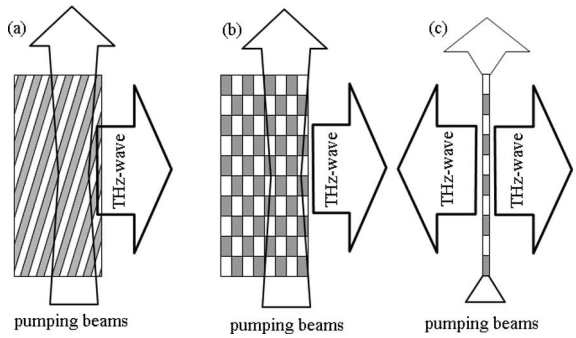

Fig. 16. Schematic of several types of PPLN for surface emitted THz-wave generation and directions THz wave goes. (a) Slanted PPLN. (b) Checkerboarded PPLN. (c) Ridged PPLN.

III. Difference-Frequency Generation Using Periodically Polled Lithium Niobate

Among the means of generating THz waves via nonlinear optical down-conversion processes, difference-frequency generation (DFG) presents great advantages [7]–[9]: it is easy to tune and affords wide tunability with high power output. However, nonlinear optical materials have high absorption coefficients in the THz-wave region, which prevents efficient THz-wave generation. Almost all THz waves generated in absorptive media disappear in the crystal. This is a major constraint for efficient THz-wave generation using nonlinear crystals. In this section, we introduce a quasi-phase-matching (QPM) technique to overcome these problems.

A. Surface-Emitting Devices

Avetisyan *et al*. proposed surface-emitting THz-wave generation by the DFG in a periodically poled lithium niobate (PPLN) waveguide [25], [26]. A surface-emitted THz wave radiates from the surface of the PPLN and propagates perpendicular to the direction of the pump beam. The absorption loss is minimized because the THz wave is generated from the PPLN surface. Moreover, the phase-matching condition can be designed using the PPLN with an appropriate grating period. A detailed explanation of surface-emitted THz-wave generation is given in [27].

By designing a QPM pattern to satisfy the phase-matching conditions in both the pump direction and perpendicular to the direction of THz-wave propagation, we realized surface-emitted THz-wave devices. Previously, we demonstrated surface-emitted THz-wave generation with two types of PPLN [27]–[30], as shown in Fig. 16(a) and (b): one was the slanted type and the other had a checkerboard pattern. For the first demonstration of surface-emitting THz-wave generation, we used slanted-type PPLN as the emitting device. The device inherently produces a THz wave in one direction only, determined by the symmetry of the slant pattern. Although THz-level oscillation induced by pumping two beams exists in the beam region, only the THz wave propagating to the right side in Fig. 16 is enhanced because the THz-level polarization in that direction is in-phase, while the THz waves propagating in the other directions disappear. Next, we prepared a checkerboard pattern

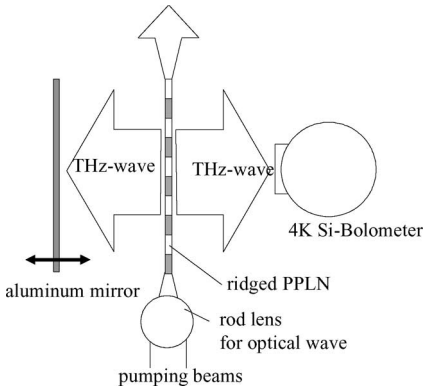

Fig. 17. Schematic of the experimental setup for generating surface-emitted THz waves using ridged PPLN and a microscopic photograph of the ridged PPLN.

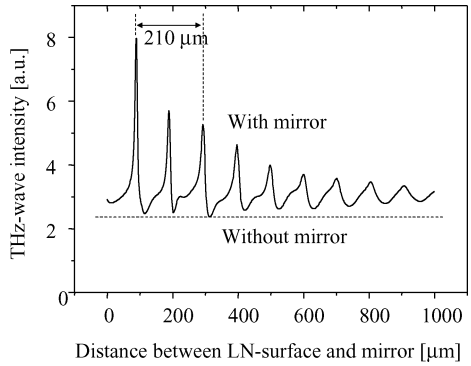

Fig. 18. THz-wave output dependence on the distance between the ridged PPLN surface and the aluminum mirror.

PPLN, such that the device had symmetry in the pumping beam and THz-wave directions. Consequently, the THz wave could propagate in any direction perpendicular to the pump beams. Although the checkerboard-patterned PPLN produces a THz wave in two directions, the THz wave propagating to the left in Fig. 16 cannot radiate outside the crystal because the absorption coefficient of lithium niobate in the THz range is very high, about 30 cm^{-1} at 1.5 THz.

In each case, the beam waist of the pump beams in the PPLN was about 140 μm, which corresponded to about four cycles of THz waves at 1.5 THz because the refractive index of lithium niobate is about 5.2. Therefore, we considered ways to satisfy phase matching in the THz-wave propagation direction. By reducing the width of the PPLN in the direction of THz-wave propagation to about one-half of the THz wavelength, that is, about 20 μm, no need existed to consider phase matching in that direction. In this study, we prepared conventional PPLN with a periodic poled domain in the x-axis direction and cut away the left side of the PPLN, except for a 20 μm ridge, as shown in Fig. 16(c) [31]. Since the ridge region had two surfaces, THz waves could be emitted from each side. The prepared PPLN had a 90-μm periodic domain period, 0.5-mm crystal thickness, and 35-mm interaction length. After fabricating the PPLN, we cut away the left side of the PPLN with a dicing saw (DAD522; Disco), giving a ridge height and thickness of about 300 and 20 μm, respectively. A smooth surface in the y-plane of the PPLN could be obtained under the proper cutting conditions. We also anticipate that the device could serve as a slab waveguide for two pump beams, maintaining a high field intensity of the pump beams throughout the interaction length.

Fig. 17 shows the experimental setup. The DFG pump source is the same as described in [30]. Two optical pulses with a 1-MHz repetition rate and 100-ps pulse duration were collimated and focused on the PPLN ridge using an $f = 100$ mm circular lens and an $r = 1$ mm rod lens, after amplifying the average power of the erbium-doped fiber amplifier (EDFA) to 1 W. The wavelengths of the two pump waves were 1554 and 1566 nm, respectively, and the corresponding THz-wave frequency was about 1.48 THz (wavelength 203 μm). The peak optical power was almost 10 kW. The THz waves travel in two directions perpendicular to the pump beam path. We expected that the THz-wave intensity would be enhanced by reflecting the THz wave going to the left and overlapping the reflected THz wave with the wave traveling to the right. The THz wave was detected using a 4 K Si bolometer to the right of the ridged PPLN, after collimating it using a rod-shaped THz-super lens (Tsurupica) 2 mm in diameter. The average power of the THz-wave output exceeded 400 pW, which corresponded to an estimated THz-wave peak power of about 4 μW. To verify the enhancement effect of reflecting and overlapping the THz waves, we placed an aluminum mirror to the left of the ridged PPLN as a THz-wave reflector. We aligned the angle of the mirror surface carefully so that it was parallel to the ridged PPLN surface and controlled the mirror position using a stepping motor with 0.1 μm resolution.

Fig. 18 shows dependence of the THz-wave intensity on the distance from the ridged PPLN surface to the mirror. A periodic structure with a period of about 105 μm, which corresponded to one-half of the THz wavelength, was observed on scanning the mirror. The amplitude of the periodic structure decreased on moving the mirror farther from the PPLN surface, and the THz-wave intensity decreased to the value without the mirror. The periodic structure of the THz wave was asymmetric, and the reason for the asymmetry is under investigation. A notable result of this demonstration was that the greatest THz-wave output was about 2.7 times greater than that without the mirror under these conditions. We measured the input–output property of the THz wave with and without the mirror. When the mirror was used, it was placed to give the most intense THz wave, around 90 μm in Fig. 18.

Fig. 19 shows the results: squares denote the THz-wave intensity without the mirror and diamonds indicate the intensity with the mirror. As the figure shows, the THz-wave intensity increased with the mirror. The THz-wave output properties without the mirror were fit by a characteristic square function, and the threshold of THz-wave generation did not appear. These results are in good agreement with well-known DFG characteristics. Conversely, the output with the mirror could not be fit by the square function, but was fit by a 3.3 power function. Considering the interferometric effect between the two THz waves, the power should be 2.0; however, the power estimated experimentally was 3.3. The result indicated that the THz wave

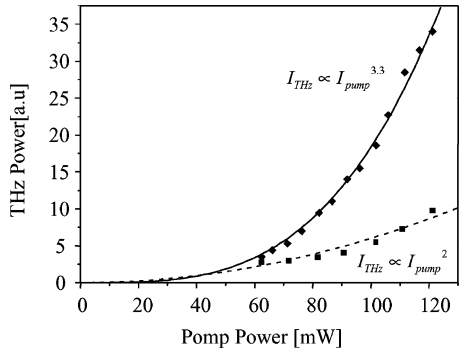

Fig. 19. Input–output property of the THz-wave intensity measured on the right side of the PPLN without (squares) and with (diamonds) a mirror to the left.

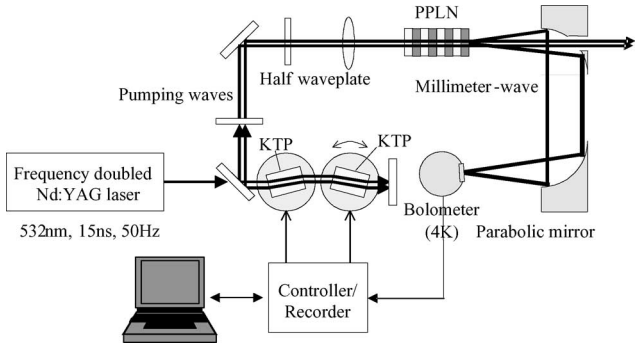

Fig. 20. Experimental setup used for millimeter wave generation.

reflected by the mirror passed through the PPLN crystal again, where it was amplified, that is, the reflected THz wave acted as a seed source for growth of the THz-level oscillation in the PPLN, which enhanced the THz polarization. We demonstrated the amplification of THz waves by ferroelectric materials. If the ridged PPLN was set in a THz-wave oscillator, such as a Fabry–Pérot interferometer consisting of two metal-mesh plates or a photonic crystal oscillator in the THz-wave region, we observed great enhancement of the THz wave. We believe that this is a promising method for generating efficient continuous THz waves [29].

B. Collinear Phase-Matching Device

For THz-wave frequencies, parametric frequency conversion using $LiNbO_3$ has been demonstrated, and compact, pulsed high-peak power sources, such as a TPO and IS-TPG, have been realized. Unfortunately, this method cannot be applied to the sub-THz wave region because the parametric process is based on noncollinear phase matching and requires a specially designed mirror or very tight alignment. For example, the idler wavelength in a parametric process should be 1064.8 nm under 1064 nm pumping (this is, the fundamental wavelength of a Nd:YAG laser and the typical wavelength for a TPO and IS-TPG), and the internal angle for phase matching between the pump and idler waves should be 0.09°. In this configuration, the fabrication of a special mirror that works for such close wavelengths, with high transmittance for the pump wave and high reflectance for the idler wave, is quite difficult. To overcome this problem, the QPM shows promise [32]. Unfortunately, the high absorbance of a nonlinear crystal prevents effective overlapping of the generated waves. The QPM technique using $LiNbO_3$ crystal (10–30 cm^{-1} absorption coefficient in the THz-wave region [12]) is not effective for THz-wave generation.

$LiNbO_3$ has a low absorption coefficient in the sub-THz wave region, and it is about 2 cm^{-1} at 200 GHz [12]. This means that the QPM technique can be used to generate sub-THz waves using PPLN crystal in the collinear phase-matching configuration. The required period was very long, about 500 μm at around 200 GHz. The poling process for such a long period is easily realized using the conventional electric field method.

$LiNbO_3$ has an absorption coefficient of about 2 cm^{-1} at 200 GHz, which results in an effective interaction length of about 70 mm. This value is the standard length used for the practical fabrication of the PPLN.

We fabricated such PPLN using the conventional electric field method on 0.5-mm-thick $LiNbO_3$ wafers. The long periodic structure was fabricated easily without fluctuations in the period and duty ratio. The interaction length of the PPLN was 40 mm; this length would seem unusual, but the conversion efficiency compared to the PPLN with a 70-mm interaction length is reduced by only 3% analytically. The polarization inversion periods of the PPLN were 396 and 300 μm, and the corresponding frequencies with those devices were 260 and 340 GHz, respectively [33].

We used a dual wavelength optical parametric oscillator (OPO) using two potassium titanium oxide phosphate (KTP) crystals as the pump source for the DFG process [34]. The second harmonic of a Q-switched Nd:YAG laser (532 nm, 15 ns, and 50 Hz) was used as the pump source for the KTP-OPO. Each KTP crystal was mounted on a Galvano-optical beam scanner and the angle was controlled independently. The KTP-OPO had a tuning range of 1300–1600 nm, and each wavelength was controllable independently. The maximum output energy of 2 mJ was obtained under 12 mJ pumping, and the estimated peak power of each wave was about 130 kW.

The experimental setup used to generate sub-THz waves is shown in Fig. 20. The output beam of the KTP-OPO was focused into a PPLN crystal, and the estimated beam waist was about 300 μm. The emitted sub-THz wave was collimated and focused onto a 4 K Si bolometer detector using parabolic mirrors. The transmitted pump waves and generated second harmonic waves passing in the PPLN passed through a hole in the first parabolic mirror. Sub-THz waves were generated successfully and detected using our system. The measured sub-THz wave spectra with fixed $\lambda_1 = 1300$ nm and tuned $\lambda_2 = 1300 \sim 1314$ nm are shown in Fig. 21. The solid and dashed curves denote the sub-THz wave spectra generated using the PPLN with inversion periods of 300 and 396 μm, respectively. The estimated frequency of the sub-THz waves considering the pumping wavelength agreed well with the designed frequencies (340 and 260 GHz with inversion periods of 300 and 396 μm, respectively). Higher order QPM also generated higher frequency waves, including THz waves.

The highest energy of an obtained sub-THz wave was about 1.43 pJ, and the estimated peak power was 0.1 mW. The PPLN

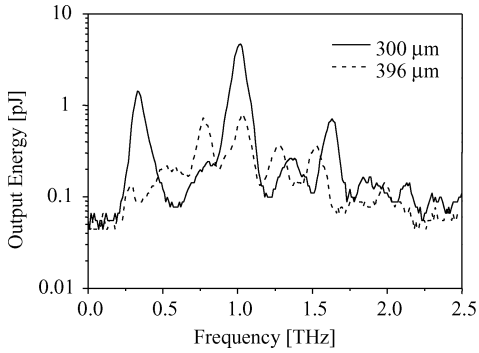

Fig. 21. Measured output spectra of the millimeter waves emitted by the PPLN with polarization periods of 396 and 300 μm.

used in this study was very thin, only 0.5 mm, and this value is comparable to the sub-THz waves generated. Diffraction of the sub-THz wave decreased the conversion efficiency, and higher pump energy could not be inserted into the PPLN to prevent crystal damage. The PPLN was not AR coated, which also reduced the efficient coupling of the pump wave into the PPLN crystal. In addition, we had used a congruent $LiNbO_3$ crystal. In general, a MgO-doped $LiNbO_3$ crystal is suitable for THz-wave generation, and approximately five times more THz-wave radiation was detected using a MgO-doped $LiNbO_3$ crystal than with a congruent $LiNbO_3$ crystal [11]. In addition, the Si bolometer used to detect sub-THz waves was optimized for THz-wave detection. The exit aperture in the Winston cone in the bolometer was 1.6 mm, which means that the cutoff frequency of the aperture was about 200 GHz. The frequency of the sub-THz waves detected in this study was comparable to the value of the cutoff frequency of the Winston cone, while the coupling efficiency was poor in such a low frequency region. In this study, we used the DFG method to generate sub-THz waves, which involved single-pass frequency conversion. The optical parametric interaction can be applied to sub-THz wave generation using the PPLN and an optical parametric oscillator, which is a promising method for highly efficient nonlinear frequency conversion. Improvement of the experimental conditions should result in sub-THz wave generation with a two to three times greater peak power.

IV. Conclusion

We reviewed widely tunable THz-wave generation based on the optical parametric process. We presented a TPO using monolithic grating couplers in Section III. Tunability, coherency, power, polarization, radiation angle, and divergence were measured, verifying that this method is suitable for many purposes, including spectroscopy, communication, medical and biological applications, and THz imaging. Section IV presented an efficient TPO that introduced an arrayed Si-prism coupler. The output was more than six times greater than with single-prism coupling. The diffraction angle observed using the prism array was smaller than with single-prism coupling because of the phased-array-like effect. Furthermore, we discussed the unidirectional THz-wave radiation from the Si-prism coupler. Using difference frequency generating method of periodically poled $LiNbO_3$ crystal, higher conversion efficiency has been achieved and continuous wave operation of THz-wave generation was realized.

Acknowledgment

The authors thank T. Shibuya, Dr. H. Minamide, Dr. K. Imai and Prof. H. Ito of RIKEN and Prof. Y. Avetisyan of the Microwave Engineering Department, Yerevan State University, Dr. J. Shikata of the Research Institute of Electrical Communication, Tohoku University, for useful discussions; Prof. K. Mizuno of the Research Institute of Electrical Communication, Tohoku University, for providing the Schottky barrier diodes; Dr. S. Sasaki and Y. Suzuki of the Research Institute of Electrical Communication, Tohoku University and T. Akiba of the Department of Electrical Engineering, Nagoya University, for their experimental support for the part of the work; Prof. H. Yokoyama, for grateful help for using compact pulsed diode laser; Dr. S. Nagano and Prof. K. Edamatsu of the Research Institute of Electrical Communication, for fabricating PPLN crystals; C. Takyu for his excellent work coating the crystal surface, and T. Shoji for polishing the crystals superbly.

References

[1] D. M. Mittleman, M. Gupta, R. Neelamani, R. G. Baraniuk, J. V. Rudd, and M. Koch, "Recent advances in terahertz imaging," *Appl. Phys. B Lasers Opt.*, vol. 68, no. 6, pp. 1085–1094, Jun. 1999.

[2] F. Zernike and P. R. Berman, "Generation of far infrared as a difference frequency," *Phys. Rev. Lett.*, vol. 15, no. 26, pp. 999–1001, Dec. 1965.

[3] J. R. Morris and Y. R. Shen, "Theory of far-infrared generation by optical mixing," *Phys. Rev. A*, vol. 15, no. 3, pp. 1157–1168, Mar. 1977.

[4] J. M. Yarborough, S. S. Sussman, H. E. Purhoff, R. H. Pantell, and B. C. Johnson, "Efficient, tunable optical emission from $LiNbO_3$ without a resonator," *Appl. Phys. Lett.*, vol. 15, no. 5, pp. 102–105, Aug. 1969.

[5] B. C. Johnson, H. E. Puthoff, J. SooHoo, and S. S. Sussman, "Power and linewidth of tunable stimulated far-infrared emission in $LiNbO_3$," *Appl. Phys. Lett.*, vol. 18, no. 5, pp. 181–183, Mar. 1971.

[6] M. A. Piestrup, R. N. Fleming, and R. H. Pantell, "Continuously tunable submillimeter wave source," *Appl. Phys. Lett.*, vol. 26, no. 8, pp. 418–421, Apr. 1975.

[7] G. D. Boyd, T. J. Bridges, C. K. N. Patel, and E. Buehler, "Phase-matched submillimeter wave generation by difference-frequency mixing in $ZnGeP_2$," *Appl. Phys. Lett.*, vol. 21, no. 11, pp. 553–555, Dec. 1972.

[8] W. Shi, Y. J. Ding, N. Fernelius, and K. Vodopyanov, "Efficient, tunable, and coherent 0.18–5.27-THz source based on GaSe crystal," *Opt. Lett.*, vol. 27, no. 16, pp. 1454–1456, Aug. 2002.

[9] T. Tanabe, K. Suto, J. Nishizawa, K. Saito, and T. Kimura, "Tunable terahertz wave generation in the 3- to 7-THz region from GaP," *Appl. Phys. Lett.*, vol. 83, pp. 237–239, Jul. 2003.

[10] I. Shoji, T. Kondo, A. Kitamoto, M. Shirane, and R. Ito, "Absolute scale of second-order nonlinear-optical coefficients," *J. Opt. Soc. Amer. B*, vol. 14, no. 9, pp. 2268–2294, Sep. 1997.

[11] J. Shikata, K. Kawase, K. Karino, T. Taniuchi, and H. Ito, "Tunable terahertz-wave parametric oscillators using $LiNbO_3$ and MgO:$LiNbO_3$ crystals," *IEEE Trans. Microw. Theory Tech.*, vol. 48, no. 4, pp. 653–661, Apr. 2000.

[12] E. D. Palik, *Handbook of Optical Constants of Solids,* vols. I and II. New York: Academic, 1998.

[13] K. Kawase, M. Sato, T. Taniuchi, and H. Ito, "Coherent tunable THz-wave generation from $LiNbO_3$ with monolithic grating coupler," *Appl. Phys. Lett.*, vol. 68, no. 18, pp. 2483–2485, Apr. 1996.

[14] K. Kawase, M. Sato, T. Taniuchi, and H. Ito, "Characteristics of THz-wave radiation using a monolithic grating coupler on a $LiNbO_3$ crystal," *Int. J. Infrared Millim. Waves*, vol. 17, no. 11, pp. 1839–1849, Nov. 1996.

[15] T. Nozokido, J. J. Chang, C. M. Mann, T. Suzuki, and K. Mizuno, "Optimization of a Schottky barrier mixer diode in the submillimeter wave region," *Int. J. Infrared Millim. Waves*, vol. 15, no. 11, pp. 1851–1865, Nov. 1994.

[16] J. Shikata, K. Kawase, M. Sato, K. Nakamura, T. Taniuchi, and H. Ito, "Enhancement of terahertz-wave output from $LiNbO_3$ optical parametric oscillators by cryogenic cooling," *Opt. Lett.*, vol. 24, no. 4, pp. 202–204, Feb. 1999.
[17] K. Kawase, K. Nakamura, M. Sato, T. Taniuchi, and H. Ito, "Unidirectional radiation of widely tunable THz wave using a prism coupler under noncollinear phase matching condition," *Appl. Phys. Lett.*, vol. 71, no. 6, pp. 753–755, Aug. 1997.
[18] K. Kawase, J. Shikata, H. Minamide, K. Imai, and H. Ito, "Arrayed silicon prism coupler for a terahertz-wave parametric oscillator," *Appl. Opt.*, vol. 40, no. 9, pp. 1423–1426, Mar. 2001.
[19] T. Nozokido, H. Minamide, and K. Mizuno, "Modulation of submillimeter wave radiation by laser-produced free carriers in semiconductors," *Electron. Commun. Jpn.,* Part 2, vol. 80, no. 6, pp. 1–9, 1997.
[20] K. Kawase, J. Shikata, K. Imai, and H. Ito, "Transform-limited, narrow-linewidth, terahertz-wave parametric generator," *Appl. Phys. Lett.*, vol. 78, no. 19, pp. 2819–2821, May 2001.
[21] K. Kawase, H. Minamide, K. Imai, J. Shikata, and H. Ito, "Injection-seeded terahertz-wave parametric generator with wide tenability," *Appl. Phys. Lett.*, vol. 80, no. 2, pp. 195–197, Jan. 2002.
[22] K. Kawase, J. Shikata, and H. Ito, "Terahertz wave parametric source," *J. Phys. D: Appl. Phys.*, vol. 35, no. 3, pp. R1–R14, Jan. 2002.
[23] S. Wu, V. A. Kapinus, and G. A. Blake, "A nanosecond optical parametric generator/amplifier seeded by an external cavity diode laser," *Opt. Commun.*, vol. 159, no. 1–3, pp. 74–79, Jan. 1999.
[24] K. Imai, K. Kawase, J. Shikata, H. Minamide, and H. Ito, "Injection-seeded terahertz-wave parametric oscillator," *Appl. Phys. Lett.*, vol. 78, no. 8, pp. 1026–1028, Feb. 2001.
[25] Y. Avetisyan and K. Kocharyan, "A new method of terahertz difference frequency generation using periodically poled waveguide," in *Proc. Conf. Lasers Electro-Opt., OSA 1999 Tech. Dig.*, May, pp. 380–381.
[26] Y. Avetisyan, Y. Sasaki, and H. Ito, "Analysis of THz-wave surface-emitted difference-frequency generation in periodically poled lithium niobate waveguide," *Appl. Phys. B*, vol. 73, pp. 511–514, 2001.
[27] Y. Sasaki, Y. Avetisyan, K. Kawase, and H. Ito, "Terahertz-wave surface-emitted difference frequency generation in slant-stripe-type periodically poled $LiNbO_3$ crystal," *Appl. Phys. Lett.*, vol. 81, no. 18, pp. 3323–3325, Oct. 2002.
[28] Y. Sasaki, H. Yokoyama, and H. Ito, "Dual-wavelength optical-pulse source based on diode lasers for high-repetition-rate, narrow bandwidth terahertz-wave generation," *Opt. Exp.*, vol. 12, no. 14, pp. 3066–3071, Jul. 2004.
[29] Y. Sasaki, H. Yokoyama, and H. Ito, "Surface-emitted continuous-wave terahertz radiation using periodically poled lithium niobate," *Electron. Lett.*, vol. 41, no. 12, pp. 712–713, Feb. 2005.
[30] Y. Sasaki, Y. Avetisyan, H. Yokoyama, and H. Ito, "Surface-emitted terahertz-wave difference frequency generation in two-dimensional periodically poled lithium niobate," *Opt. Lett.*, vol. 30, no. 21, pp. 2927–2929, Nov. 2005.
[31] K. Suizu, Y. Suzuki, Y. Sasaki, H. Ito, and Y. Avetisyan, "Surface-emitted terahertz-wave generation by ridged periodically poled lithium niobate and enhancement by mixing of two terahertz waves," *Opt. Lett.*, vol. 31, no. 7, pp. 957–959, Apr. 2006.
[32] J. A. Armstrong, N. Bloembergen, J. Ducuing, and P. S. Pershan, "Interactions between light waves in a nonlinear dielectric," *Phys. Rev.*, vol. 127, no. 6, pp. 1918–1939, Sep. 1962.
[33] K. Suizu, T. Shibuya, S. Nagano, T. Akiba, K. Edamatsu, H. Ito, and K. Kawase, "Pulsed high peak power millimeter wave generation via difference frequency generation using periodically poled lithium niobate," *Jpn. J. Appl. Phys.*, vol. 46, no. 40, pp. L982–L984, Oct. 2007.
[34] H. Ito, K. Suizu, T. Yamashita, T. Sato, and A. Nawahara, "Random frequency accessible broad tunable terahertz-wave source using phase-matched 4-dimethylamino-N-methyl-4-stilbazolium tosylate crystal," *Jpn. J. Appl. Phys.*, vol. 46, no. 11, pp. 7321–7324, Nov. 2007.

Koji Suizu was born in Fukuoka, Japan, in 1974. He received the B.S. degree in physics, and the M.S. and Ph.D. degrees in applied physics from Kyushu University, Fukuoka, Japan, in 1996, 1998, and 2001, respectively.

In 2001, he joined the Tera-Photonics Project of the Photo Dynamics Research Center (PDC), RIKEN, Sendai, Japan. In 2003, he was a Research Associate with the Research Institute of Electrical Communication, Tohoku University, Sendai. In 2006, he joined the Department of Electrical Engineering, Nagoya University, Nagoya, Japan, where he is currently an Assistant Professor. His current research interests include tunable coherent terahertz generation based on nonlinear optics and their application.

Kodo Kawase (M'02) was born in Kyoto, Japan, in 1966. He received the B.S. degree in electronic engineering from Kyoto University, Kyoto, in 1989, and the M.S. and Ph.D. degrees in electronic engineering from Tohoku University, Sendai, Japan, in 1992 and 1996, respectively.

In 1998, he was an Assistant Professor at Tohoku-Gakuin University, Sendai. In 1999, he became a Subteam Leader at Photo Dynamics Research Center, RIKEN, Sendai. Thereafter, he was a Leader of Kawase Initiative Research Unit at RIKEN, in 2001. During 2004, he was a Professor in the Graduate School of Agricultural Science, Tohoku University. Since July 2005, he is a Professor in the Graduate School of Engineering, Nagoya University, Nagoya, Japan, and is also affiliated with RIKEN. His current research interests include terahertz wave generation and its applications.